The Tearing Instability of Resistive Magnetohydrodynamics

David MacTaggart

School of Mathematics & Statistics, University of Glasgow, UK

Abstract In this Chapter we explore the linear onset of one of the most important instabilities of resistive magnetohydrodynamics, the tearing instability. In particular, we focus on two important aspects of the onset of tearing: asymptotic (modal) stability and transient (non-modal) stability. We discuss the theory required to understand these two aspects of stability, both of which have undergone significant development in recent years.

1 Introduction

The terms *resistive* and *non-ideal* magnetohydrodynamics (MHD) are often used interchangedly. However, there is an important distinction. Consider Ohm's law

$$\mathbf{E} + \mathbf{u} \times \mathbf{B} = \mathbf{G}, \tag{1}$$

where $\mathbf{E}$ is the electric field, $\mathbf{u}$ is the velocity field, $\mathbf{B}$ is the magnetic induction field (hereafter referred to as the *magnetic field*) and $\mathbf{G}$ represents different possible terms that can be included in an "extended" Ohm's law. If $\mathbf{G} = \mathbf{0}$, then equation (1) is Ohm's law for *ideal* MHD. Ideal MHD has many interesting topological properties, one of the most famous is known as Alfvén's frozen flux theorem.

Theorem 1.1. *Let S be a material surface in a fluid governed by ideal MHD. Then*

$$\frac{\mathrm{d}}{\mathrm{d}t}\int \mathbf{B}\cdot\mathbf{n}\,\mathrm{d}S = 0, \tag{2}$$

where $\mathbf{n}$ is the normal of the surface S.

Corollary 1.2. *If a magnetic field line and a material line coincide at any instant in time, they must coincide for all time.*

The proofs of these statements can be found in many MHD textbooks (e.g. Biskamp, 1993; Schindler, 2006), so we do not reproduce them here. Putting these results into words, however, *in ideal MHD, the magnetic field changes as if field lines were "frozen into the fluid"*. This property means that for any flow field, the topology (or connectivity) of the magnetic field remains unchanged.

It can be shown that non-ideal forms of Ohm's law (i.e. $\mathbf{G} \neq \mathbf{0}$) can also preserve the topology of magnetic field lines. The most general form of $\mathbf{G}$ which achieves this is

$$\mathbf{G} = \mathbf{H} + \mathbf{u}' \times \mathbf{B}, \quad \nabla \times \mathbf{H} = \lambda \mathbf{B}, \tag{3}$$

for a "new" velocity field $\mathbf{u}'$ and a scalar λ (e.g. Newcomb, 1958; Priest and Forbes, 1993; Birn and Priest, 2007; Schindler, 2006). Several physical quantities that normally appear in an extended Ohm's law take the form of (3). For example, if we include the Hall term on the right-hand side of equation (1), we have

$$\mathbf{E} + \mathbf{u} \times \mathbf{B} = \beta(\nabla \times \mathbf{B}) \times \mathbf{B}, \tag{4}$$

where β is a constant. By writing $\mathbf{v} = \mathbf{u} - \beta \nabla \times \mathbf{B}$ we return to the ideal Ohm's law (2) with the flow field $\mathbf{u}$ replaced by a new transport velocity $\mathbf{v}$. Many more details of the extended Ohm's law will be considered in Chapter 3.

If, instead, we choose $\mathbf{G} = \eta \nabla \times \mathbf{B}$, where η is called the *magnetic diffusivity*, we have *resistive* MHD. This version of Ohm's law is non-ideal and does not preserve magnetic flux or field line topology except in very special circumstances (e.g. Jette, 1970). Combining the resistive Ohm's law with Maxwell's equations of electromagnetism leads to the resistive induction equation

$$\frac{\partial \mathbf{B}}{\partial t} = \nabla \times (\mathbf{u} \times \mathbf{B}) + \eta \nabla^2 \mathbf{B}, \tag{5}$$

for constant η. When $\eta \gg 1$ it does not really make sense to speak of magnetic topology as the field lines diffuse through the fluid on all scales. When $\eta \ll 1$, as in almost all astrophysical applications, the magnetic field will behave as if it followed ideal MHD except in (generally small) regions where there is strong current density. Such locations are where *magnetic reconnection* takes place, i.e. the changing of the topology of the magnetic field.

Since current density in MHD is given by $\mathbf{j} = \mu^{-1} \nabla \times \mathbf{B}$, where μ is the magnetic permeability of free space, high current density corresponds to

regions where the magnetic field has "high curl". One situation where this is produced is in regions where the magnetic field changes direction rapidly, on a length scale much smaller than the global length scale of the system, forming sheets of high current density known as *current sheets*. Current sheets have often been defined as discontinuous surfaces in ideal MHD (see Chapter 1). In this Chapter we consider current sheets with *finite thickness*, which is physically more realistic and, as will be made clear, important for stability analysis.

The rest of this Chapter will focus on the linear stability of current sheets. When a current sheet is unstable, magnetic islands (or plasmoids in three dimensions) form via reconnection. Due to this behaviour, the instability is known as the *tearing instability* (TI). Our analysis of the onset of the TI will be split in two. The first part will focus on asymptotic (or modal) stability and is, by far, the most studied description of stability. The second part will consider transient (or non-modal) growth, which has been studied less than modal stability but can be of significant importance for a complete description of the onset of the TI.

2 Asymptotic stability

2.1 The classical results

We will now present some classical results of the TI onset which stem from the seminal work of Furth et al. (1963). Although this topic has been treated in several textbooks (e.g. Priest and Forbes, 1993; Schindler, 2006; Goedbloed et al., 2010) we include a brief description here for completeness and to set the scene for later discussions related to both asymptotic stability and transient growth.

To study the TI, we consider the two-dimensional (2D) incompressible MHD equations

$$\rho\left(\frac{\partial \mathbf{u}}{\partial t} + (\mathbf{u}\cdot\nabla)\mathbf{u}\right) = -\nabla p + \mu^{-1}(\nabla\times\mathbf{B})\times\mathbf{B}, \tag{6}$$

$$\frac{\partial \mathbf{B}}{\partial t} = \nabla\times(\mathbf{u}\times\mathbf{B}) + \eta\nabla^2\mathbf{B}, \tag{7}$$

$$\nabla\cdot\mathbf{B} = \nabla\cdot\mathbf{u} = 0, \tag{8}$$

where $\mathbf{B}$ and $\mathbf{u}$ are as defined previously, ρ is the (constant) density, p is the plasma pressure, η is the constant magnetic diffusivity and μ is the magnetic permeability.

For our background (static) equilibrium,

$$p_0 = p_0(x), \quad \mathbf{B}_0 = B_{0z}(x)\mathbf{e}_z, \quad \mathbf{u}_0 = \mathbf{0}. \tag{9}$$

where the subscript 0 corresponds to the equilibrium and

$$p_0(x) + \frac{1}{2\mu}B_{0z}^2(x) = \text{const.} \tag{10}$$

Before choosing a particular form for $B_{0z}(x)$, let us linearize the MHD equations. Setting $(\mathbf{u}, \mathbf{B}, p) = (\mathbf{u}_0, \mathbf{B}_0, p_0) + (\mathbf{u}_1, \mathbf{B}_1, p_1)$ leads to the linearization

$$\rho\frac{\partial \mathbf{u}_1}{\partial t} = -\nabla p_1 + \mu^{-1}(\nabla \times \mathbf{B}_1) \times \mathbf{B}_0 + \mu^{-1}(\nabla \times \mathbf{B}_0) \times \mathbf{B}_1, \tag{11}$$

$$\frac{\partial \mathbf{B}_1}{\partial t} = \nabla \times (\mathbf{u}_1 \times \mathbf{B}_0) + \eta\nabla^2\mathbf{B}_1 \tag{12}$$

$$\nabla \cdot \mathbf{B}_1 = \nabla \cdot \mathbf{u}_1 = 0. \tag{13}$$

Note that we are assuming $\eta \ll 1$ which is typical in many solar and astrophysical applications. We therefore ignore the contribution of diffusion on the background equilibrium in equation (12), expecting the dynamics of the instability to to occur on a much shorter time scale than the diffusion time. For a discussion on the influence of background diffusion, the reader is directed to Dobrott et al. (1977).

We now look for solutions of the form

$$\mathbf{u}_1 = [u(x,t), 0, u_z(x,t)]^T e^{ikz}, \quad \mathbf{B}_1 = [b(x,t), 0, b_z(x,t)]^T e^{ikz}, \tag{14}$$

where k is the wavenumber of disturbances in the z-direction. Taking the curl of equation (11), we eliminate p_1. Using the solenoidal constraints in equation (13), we can eliminate u_z and b_z. This leaves equations

$$\frac{\partial}{\partial t}\left(\frac{\partial^2 u}{\partial x^2} - k^2 u\right) = \frac{ikB_{0z}}{\mu\rho}\left(\frac{\partial^2 b}{\partial x^2} - k^2 b\right) - \frac{ikB_{0z}{}''}{\mu\rho}b, \tag{15}$$

$$\frac{\partial b}{\partial t} = ikB_{0z}u + \eta\left(\frac{\partial^2 b}{\partial x^2} - k^2 b\right). \tag{16}$$

Primes denote differentiation with respect to x in the equilibrium magnetic field.

Equilibrium We choose a classic form for the background magnetic field known as the *Harris sheet* (Harris, 1962). The magnetic field of the Harris sheet is given by

$$B_{0z}(x) = B_0 \tanh\left(\frac{x}{a}\right), \quad {B_{0z}}''(x) = -\frac{B_0}{a^2}\frac{2}{\cosh^2(x/a)}\tanh\left(\frac{x}{a}\right), \tag{17}$$

where B_0 is the maximal field strength and a measures the thickness of the current sheet. The equilibrium pressure then comes from (10) but is not important for our calculations.

Nondimensionalization To non-dimensionalize the equations, consider

$$u = u_0 u^*, \quad b = B_0 b^*, \quad t = t_0 t^*, \quad x = a x^*. \tag{18}$$

Further, if we take

$$t_0 = \frac{a}{u_0} := \tau_A, \quad u_0 = \frac{B_0}{\sqrt{\mu\rho}} := u_A, \tag{19}$$

where the latter is the Alfvén speed, the linearized MHD equations become (after dropping the *s)

$$\frac{\partial}{\partial t}\left(\frac{\partial^2 u}{\partial x^2} - k^2 u\right) = ikB_{0z}\left(\frac{\partial^2 b}{\partial x^2} - k^2 b\right) - ik{B_{0z}}'' b, \tag{20}$$

$$\frac{\partial b}{\partial t} = ikB_{0z}u + \frac{1}{S}\left(\frac{\partial^2 b}{\partial x^2} - k^2 b\right), \tag{21}$$

where

$$S = \frac{a u_0}{\eta}, \tag{22}$$

is the non-dimensional constant known as the *Lundquist* number. Note that in order not to introduce unnecessary new notation, B_{0z} now represents the non-dimensionalized quantity in $(17)_1$.

Assuming a time dependence of $\exp(\sigma t)$, the equations describing the classical linear onset of the TI are

$$\sigma\left(\frac{\partial^2 u}{\partial x^2} - k^2 u\right) = ikB_{0z}\left(\frac{\partial^2 b}{\partial x^2} - k^2 b\right) - ik{B_{0z}}'' b, \tag{23}$$

$$\sigma b = ikB_{0z}u + \frac{1}{S}\left(\frac{\partial^2 b}{\partial x^2} - k^2 b\right). \tag{24}$$

d	5	10	15	20	25
σ	0.01059	0.01307	0.01309	0.01309	0.01309

Table 1. Tearing mode growth rate, for $k = 0.5$ and $S = 1000$, as a function of the domain size d.

The assumption of a time dependence of $\exp(\sigma t)$ is a standard step in linear stability theory and has been made in many linear stability studies throughout the past century. However, this simple step has a profound influence on the description of the linear onset of an instability. Indeed, it is the reason why this section is entitled "Asymptotic stability". We will discuss this point in more detail in Section 3.

As mentioned earlier, resistive effects are often only important in small regions, especially when $S \gg 1$. Outside of these regions, the behaviour of the fluid can be described by ideal MHD. The classical approach of determining the growth rate σ in equations (23) and (24) is based on the identification of a (thin) resistive region (current sheet) and an ideal region (far from the current sheet). Using the method of *matched asymptotic expansions* (e.g. Eckhaus, 1973; Van Dyke, 1975), the solution behaviour in both regions can be matched, allowing for a dispersion relation to be found. This approach has been reproduced, in excellent detail, in many textbooks (e.g. Schindler, 2006; Goedbloed et al., 2010) and so here we will only highlight the most important details of the dispersion relation needed for later in the Chapter.

We solve equations (23) and (24) numerically (MacTaggart and Stewart, 2017; MacTaggart, 2018) with no-slip and perfectly conducting boundary conditions,

$$u = b = 0 \quad \text{at } z = \pm d, \tag{25}$$

where d is a non-dimensional distance. Since the tearing instability grows in a thin boundary layer at $x = 0$, the choice of boundary conditions does not have a large effect on the initial development of the instability if d is sufficiently large. As evidence of this, Table 1 displays how the growth rate of the tearing mode changes as a function of d for $S = 1000$ and $k = 0.5$.

From the numerical solution of equations (23) and (24) with boundary conditions (25), we can determine how the tearing mode growth rate varies in the (S, k) parameter space. Figure 1 displays the tearing mode dispersion relation (σ against k) for various values of S. It is noted that the eigenvalue corresponding to the growth rate of the tearing mode is purely real.

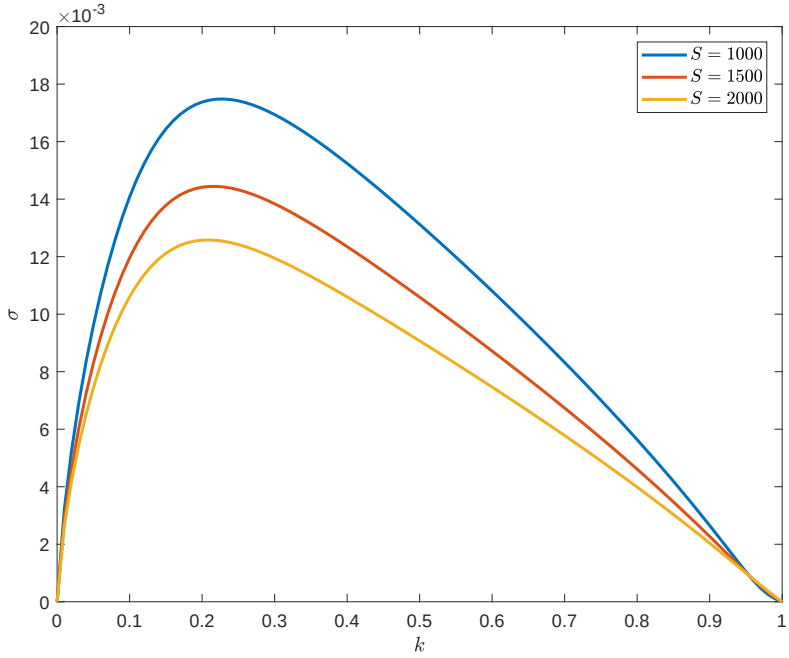

Figure 1. The dispersion relation of the tearing mode for various S.

From inspection of the numerical results, some of which are displayed in Figure 1, or from asymptotic analysis (e.g. Furth et al., 1963; Paris, 1984; Schindler, 2006; Goedbloed et al., 2010), the maximum growth rate of the tearing mode scales as

$$\sigma = O(S^{-1/2}), \quad k = O(S^{-1/4}). \tag{26}$$

For larger $k < 1$, the growth rate scales as

$$\sigma = O(S^{-3/5}). \tag{27}$$

Figure 2 displays numerically determined growth rates and how they follow, linearly, the scalings given in (26) and (27).

2.2 The plasmoid instability

In the previous section we demonstrated that the growth rate of the TI is a negative power of the Lundquist number S. This fact was originally

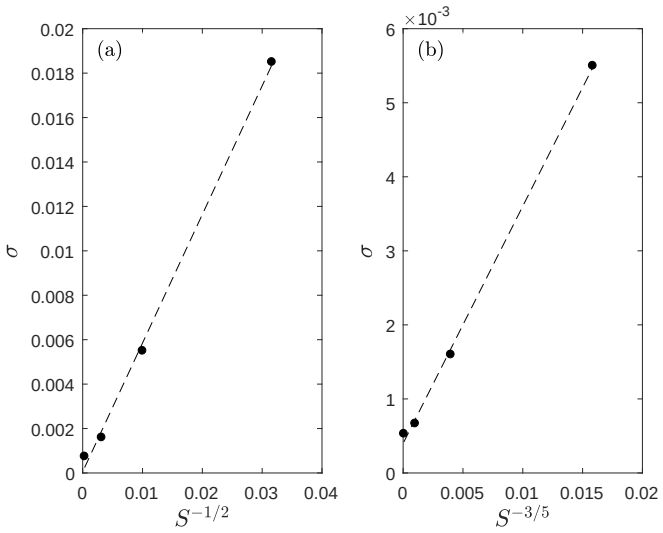

Figure 2. The tearing mode growth rate scale dependence. (a) shows the maximum value of the growth rate scaling as $S^{-1/2}$. (b) shows the growth rate for $k = 0.8$, scaling as $S^{-3/5}$. The dashed lines are lines of best fit.

perceived as a stumbling block for the application of the TI to explain examples of "fast" reconnection, such as solar flares (e.g. Priest, 1983), where $S \gg 1$. A definition of "fast" in this context corresponds to a rate greater than the Sweet-Parker rate, which we will introduce shortly.

Fast growth is, however, possible for the TI and is often referred to as the *plasmoid instability* (PI). In the linear phase of the PI, "fast" implies a growth rate that is either independent of S or is a positive power of S. Before describing the PI, we will introduce some nomenclature that is common in the TI and PI literature.

Sweet-Parker current sheet Much of the theory of magnetic reconnection is described in terms of *Sweet-Parker reconnection*. This model describes steady-state magnetic reconnection and contains a current sheet with inflow perpendicular to the sheet and parallel outflow (Parker, 1957a,b; Sweet, 1958). This model has been treated in many textbooks, so we will only provide a very brief description here. Consider the magnetic field of a null point which has been compressed into a current sheet of a particular aspect ratio with thickness a and length L. This deformation is illustrated

in Figure 3.

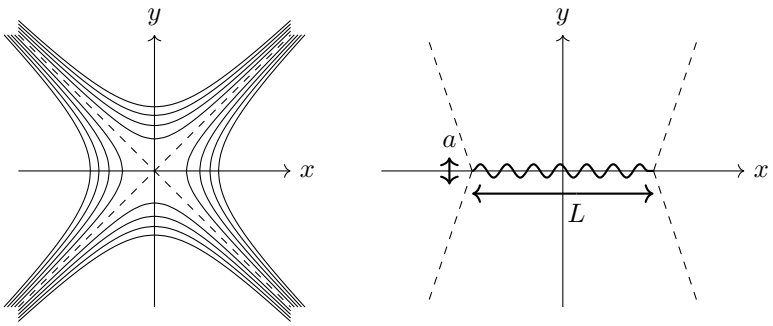

Figure 3. A schematic representation of a null point and its deformed state as a current sheet. Separatrices are dashed lines and the current sheet is represented by a crinkled line.

Assume that after the deformation, the system reconnects in a steady-state manner. If u_i is the inflow speed and u_o is the outflow speed, the Sweet-Parker model predicts

$$\frac{u_i}{u_o} = O\left(\frac{a}{L}\right) = O(S^{-1/2}). \tag{28}$$

Therefore, the steady-state reconnection rate scales as the aspect ratio of the current sheet which scales as $S^{-1/2}$. Just like the tearing mode growth rate, the steady-state rate is slow for many astrophysical problems. Although other steady-state models can produce faster reconnection rates (e.g. Petschek, 1964; Kulsrud, 2001) we will not consider them here. Instead, for our purposes, a Sweet-Parker (SP) current sheet will refer to one with the aspect ratio given in (28).

Approaches to "fast" reconnection One way to obtain faster reconnection rates is to include more physics (beyond resistive MHD) in the TI description, e.g. the Hall term (Terasawa, 1983). The Geospace Environment Challenge, or GEM Challenge, (Birn et al., 2001; Birn and Hesse, 2001) compares a variety of different codes containing different dissipation models (resistive MHD, Hall MHD, hybrid and kinetic), all applied to the same problem - a perturbed Harris sheet. The perturbation used, however, is of the same thickness as the initial current sheet, so this study does not capture the linear phase of the TI and starts in a nonlinear phase. The

result of this study is that the reconnection rate of all models is comparable except resistive MHD, which is much smaller than the rest. A similar study, known as the Newton Challenge, was carried out in order to include the formation of the thin current sheet in the simulations, rather than inserting it as an initial condition. Again, fast reconnection is found to be essentially independent of the dissipation mechanism.

Another path to producing faster dynamics is to create many small length scales (i.e. current sheets within current sheets) in which reconnection can occur and become more efficient. One way of achieving this is to include the effects of turbulence in current sheets to generate these small length scales (e.g. Lazarian and Vishniac, 1999; Shibata and Tanuma, 2001; Loureiro et al., 2009; Lazarian et al., 2015). This topic will be considered in Chapter 6. Here, we will focus on the linear phase of the PI, which can lead to the formation of small scales through the creation of many plasmoids.

Plasmoid instability The classical TI of resistive MHD, without extra physics, does posses fast dynamics, both in the linear and non-linear phases. Hints of this fast behaviour (the PI) can be found in early simulations of the TI (e.g. Forbes and Priest, 1983; Steinolfson and van Hoven, 1984; Biskamp, 1986). These simulations found that thin (SP) current sheets would always (in particular parameter regimes) become subject to the TI. However, it was not until recently that the full potential of the PI began to be uncovered. Loureiro et al. (2007) performed a linear stability analysis, similar to that of the previous section, for a thinning current sheet, i.e. a current sheet compressed by a background stagnation point flow. In their analysis, they find that the growth rate of tearing is $O(S^{1/4})$ with $S \gg 1$ in a current sheet with the SP scaling. This result has been reproduced in simulations (e.g. Bhattacharjee et al., 2009; Samtaney et al., 2009; Huang et al., 2017) which also reveal the formation of many plasmoids.

The PI is thus the TI in current sheets of a large aspect ratio and is fast since the linear growth rate is a positive power of S rather than a negative power as in the classical analysis. These results imply that once current sheets are compressed to a certain aspect ratio, they succumb to the PI and break up in the chaotic formation of plasmoids. The theory of the plasmoid instability is described in detail in Uzdensky and Loureiro (2016). Pucci and Velli (2014) argue that the SP scaling may never be reached as the onset of the PI can occur in much thicker current sheets. We now follow their argument by making use of the results for the classical onset of the TI.

First, let us assume that the aspect ratio of the current sheet follows the

scaling

$$\frac{a}{L} = O(S_L^{-\alpha}), \tag{29}$$

where $\alpha \in \mathbb{R}$ and $S_L = Lu_A/\eta$, that is the Lundquist number based on the macroscopic scale L rather than the sheet thickness a. As mentioned in the analysis of the classical TI, we are only interested in behaviour on a time scale much shorter than the global magnetic diffusion time scale. For the above aspect ratio, this time scale is

$$\tau = O(S_L^{1-2\alpha}). \tag{30}$$

Hence, we have have the constraint of considering $\alpha \lesssim 1/2$. Note that $\alpha = 1/2$ is the SP scaling that appears throughout the TI literature and can be thought of as an upper bound for α. Now, if we perform the non-dimensionalization of equations (15) and (16) where the only scaling that we change is the time scale $t_0 = L/u_A$ (i.e. the time scale is now based on the macroscopic length) and convert the equations to an eigenvalue problem, we can derive the non-dimensional equations

$$\widetilde{\sigma}\left(\frac{\partial^2 u}{\partial x^2} - k^2 u\right) = ikB_{0z}\left(\frac{\partial^2 b}{\partial x^2} - k^2 b\right) - ikB_{0z}{}'' b, \tag{31}$$

$$\widetilde{\sigma} b = ikB_{0z} u + \frac{1}{Q}\left(\frac{\partial^2 b}{\partial x^2} - k^2 b\right), \tag{32}$$

where $\widetilde{\sigma} = S_L^{-\alpha}\sigma$ and $Q = S_L^{1-\alpha}$. Notice that equations (31) and (32) are identical to equations (23) and (24) with the substitutions of $\widetilde{\sigma}$ for σ and Q for S. This means that we can use the solutions of equations (23) and (24) for equations (31) and (32). It should be noted that these equations are not strictly in the SP framework, i.e. they are one-dimensional and there is no length scale L arising naturally from the geometry of the current sheet (although Janicke (1980) shows that weak two-dimensionality does not strongly affect the classical analysis). Here we will assume that L is much larger than a, following the scaling in (29).

As described in the previous section, the maximum growth rate γ for the classical TI, as $S \gg 1$, is given by

$$\gamma = O(S^{-1/2}). \tag{33}$$

Therefore, the corresponding relation for equations (31) and (32) is

$$\widetilde{\gamma} = O(Q^{-1/2}). \tag{34}$$

With $\widetilde{\gamma} = S_L^{-\alpha}\gamma$ and the definition of Q given above, we have after simple rearrangement,

$$\gamma = O\left(S_L^{(3\alpha-1)/2}\right). \tag{35}$$

From the expression in (35), to find a growth rate that is independent of S_L, we take $\alpha = 1/3$. For $\alpha > 1/3$, the growth rate diverges with increasing S_L. Note that for the SP current sheet ($\alpha = 1/2$), $\gamma = O(S_L^{1/4})$ which is the scaling found by Loureiro et al. (2007). Therefore, when current sheets reach the critical aspect ratio of $O(S_L^{-1/3})$, Pucci and Velli (2014) argue that the background equilibrium cannot support further laminar motion (further current sheet thinning) and the chaotic phase of the PI ensues. Pucci and Velli (2014) refer to the fastest growing mode in this scenario as the *"ideal" tearing mode* since the growth rate becomes independent of S and is fast in the sense that motion acts on an "ideal MHD" time scale rather than the slow (resistive) time scale of the classical TI.

The result in (35) moves the onset of the PI away from the SP scaling to a much smaller aspect ratio for $S_L \gg 1$. For example, in the solar corona with $S_L = O(10^{12})$, the PI could set in on a current sheet of aspect ratio $O(10^4)$ rather than a (much thinner) SP current sheet with aspect ratio $O(10^6)$. The result in (35) has been generalized to other situations, such as including viscosity (Tenerani et al., 2015), changing the background equilibrium (Pucci et al., 2018) and considering a weakly collisional plasma (Del Sarto et al., 2016).

This completes our overview of the linear onset of the TI according to asymptotic stability theory (eigenvalue analysis). Asymptotic stability says nothing about how the *spatial distribution* of the initial conditions affects the development of subsequent growth. Nor does it describe *transient growth*, which could become very large in a finite time but decay to zero on a long time scale. We now move beyond asymptotic stability to give a more complete picture of the linear onset of the TI.

3 Transient growth

Until now, the focus of the onset of the TI has been on *asymptotic stability*. We introduced this term without a detailed explanation of its meaning. In this section we will provide the meaning which relates to another aspect of the linear onset of the TI - *transient behaviour*.

3.1 A toy model

In order to introduce the mathematical tools required to understand the transient phase of the TI (which we discuss in detail in Section 3.2), we will present new concepts with the help of a very simple *toy model*. This toy model can be considered as a translation of that in Trefethen et al. (1993) and Schmid and Henningson (2001) to MHD. In a setup suitable for the TI, suppose that b resembles a component of the magnetic field and j resembles a component of the current density. Consider the linear evolution equation

$$\frac{\mathrm{d}}{\mathrm{d}t}\begin{pmatrix} b \\ j \end{pmatrix} = \begin{pmatrix} -\frac{1}{S} & 0 \\ 1 & -\frac{2}{S} \end{pmatrix}\begin{pmatrix} b \\ j \end{pmatrix}, \tag{36}$$

where S represents the Lundquist number. Clearly, equation (36) is not meant to be considered as a serious model for MHD. However, its simplicity will allow us to make analytical progress and introduce new concepts.

Looking for solutions proportional to $\exp(\sigma t)$, the eigenvalues and corresponding eigenvectors are

$$\sigma_1 = -\frac{1}{S}, \qquad \mathbf{q}_1 = \frac{1}{(1+S^2)^{1/2}}\begin{pmatrix} 1 \\ S \end{pmatrix}, \tag{37}$$

$$\sigma_2 = -\frac{2}{S}, \qquad \mathbf{q}_2 = \begin{pmatrix} 0 \\ 1 \end{pmatrix}. \tag{38}$$

Therefore, the complete solution expanded in an eigenvector basis can be written as

$$\begin{pmatrix} b \\ j \end{pmatrix} = \frac{A_0}{(1+S^2)^{1/2}}\begin{pmatrix} 1 \\ S \end{pmatrix}\exp(-t/S) + B_0\begin{pmatrix} 0 \\ 1 \end{pmatrix}\exp(-2t/S), \tag{39}$$

where A_0 and B_0 are constants to be determined from the initial conditions. Notice immediately from equation (39) that both b and j decay to zero in the limit of large t. Hence, we find that the system is *asymptotically stable*. This is the result we would obtain by applying the asymptotic stability theory of the previous section.

Although the behaviour of equation (39) is clear for large times, it is not immediately obvious how the solution behaves at earlier times. Writing equation (36) as

$$\frac{\mathrm{d}}{\mathrm{d}t}\mathbf{v} = A\mathbf{v}, \tag{40}$$

where $\mathbf{v} = (b, j)^T$ and A is the matrix given in the right-hand side of equation (36), the formal solution to the initial value problem can be written as

$$\mathbf{v} = \exp(tA)\mathbf{v}_0, \tag{41}$$

where $\mathbf{v}_0 = \mathbf{v}(0)$ is the initial condition. In order to measure the maximum possible growth, we define a growth function $G(t)$ using the square of the L_2-norm of the disturbance, i.e. $\|\mathbf{v}\|_2^2 = b^2 + j^2$. Hence, the maximum growth function has the form

$$G(t) = \sup_{\mathbf{v}_0} \frac{\|\mathbf{v}(t)\|_2^2}{\|\mathbf{v}_0\|_2^2} = \sup_{\mathbf{v}_0} \frac{\|\exp(tA)\mathbf{v}_0\|_2^2}{\|\mathbf{v}_0\|_2^2} = \|\exp(tA)\|_2^2, \tag{42}$$

where use has been made of equation (41) and the last relation holds by the definition of an induced matrix norm. The matrix exponential takes the form

$$\exp(tA) = \begin{pmatrix} \exp(-t/S) & 0 \\ (\exp(-t/S) - \exp(-2t/S))S & \exp(-2t/S) \end{pmatrix}, \tag{43}$$

and Figure 4 displays its L_2-norm (squared) versus time for different values of S.

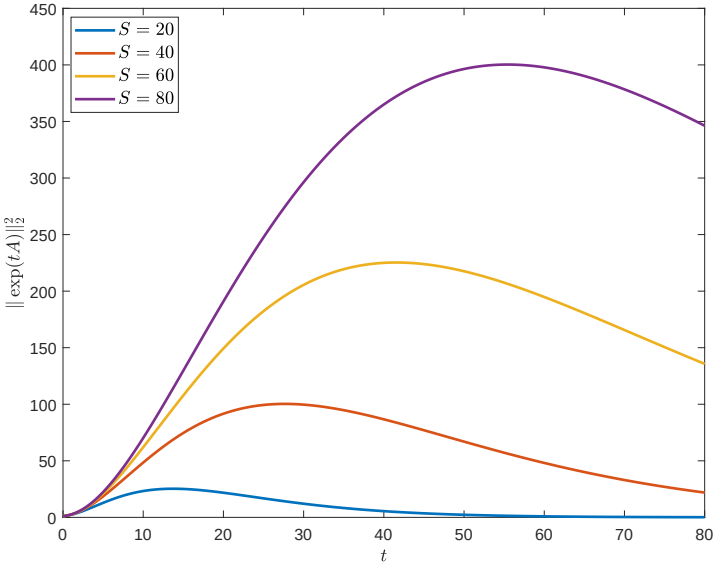

Figure 4. The growth function $G(t)$ versus t for a range of S.

What is clear from Figure 4 is that *significant growth* is possible at early times *before* the solution decays. This *transient growth* also increases with

increasing S, resulting in a possible amplification, for $S \geq 40$, of two orders of magnitude. We can make some further progress by considering the formal solution given in equations (41) and (43). If $\mathbf{v}_0 = (b_0, j_0)^T$, we have

$$b = \exp(-t/S)b_0, \tag{44}$$

and so no transient growth is possible for b. The equation for j is

$$j = (\exp(-t/S) - \exp(-2t/S))Sb_0 + \exp(-2t/S)j_0. \tag{45}$$

Transient growth is possible from the first term on the right-hand side of equation (45). Performing a Taylor series expansion of this term for $t < O(S)$,

$$\begin{aligned} (\exp(-t/S) - \exp(-2t/S))Sb_0 &= \\ \left(-\frac{t}{S} + \frac{t^2}{S^2} + \cdots + \frac{2t}{S} - \frac{4t^2}{S^2} + \ldots\right) Sb_0 &= b_0 t - \frac{3b_0}{S}t^2 + \ldots \end{aligned} \tag{46}$$

Hence, for small t, j can experience transient growth.

This transient growth is also known as *non-modal* or *algebraic* growth. These terms signify a departure from the standard normal mode analysis which is concerned with *asymptotic stability*. As we saw in the toy model, assuming a time dependence of the form $\exp(\sigma t)$ pushes the solution to a later time when the *exponential* growth or decay, controlled by the eigenvalues, dominates. Normal mode analysis does not say anything about *transient* growth that occurs on a shorter time scale and grows *algebraically*. Therefore, in order to determine a complete picture of the linear onset of an instability, we must consider the full initial value problem rather than just the eigenvalue problem. We can naturally ask, therefore, why is there so much focus on normal mode analysis which does not consider non-modal growth? A related, but more practical, question is, how can we tell if transient growth is important in a dynamical system? In order to answer this question, we will introduce some mathematical structures that will help us to determine how important transient growth can be for a particular system.

Non-normal operators In normal mode analysis, the superposition of *orthogonal* eigenfunctions leads to the linear onset of an instability being dominated by the most unstable mode determined from the associated eigenvalue problem. For the toy model, consider the normalized eigenvectors, $\mathbf{q}_1$ and $\mathbf{q}_2$. If θ is the angle between these two vectors, then

$$\cos\theta = \frac{S}{\sqrt{1+S^2}}. \tag{47}$$

It is clear that as $S \to \infty$, $\theta \to 0$. That is, these *non-orthogonal* eigenvectors tend to overlap as S increases and the eigenvector expansion becomes increasingly ill-conditioned. Since the solution depends on the superposition of *non-orthogonal* eigenvectors, even though the solution eventually decays in time, the solution can grow before it decays.

For the toy model, our eigenfunctions are just eigenvectors and the operator A is just a 2×2 matrix. Operators with non-orthogonal eigenfunctions (or eigenvectors for matrices) are known as *non-normal operators*. Normal operators have orthogonal eigenfunctions, so if a dynamical system only has normal operators then normal mode analysis will provide a full description of the linear onset of instability.

It is simple enough to determine the eigenvalues and eigenvectors of the toy model but what about more complicated systems where only a numerical solution is, perhaps, possible? In other words, how can we determine if the operator of a dynamical system is non-normal and, thus, can lead to transient growth?

ϵ-pseudospectra For problems with normal operators, as mentioned above, the eigenvalues and eigenfunctions will give all the required information about the linear stability. The spectrum of an operator A, $\sigma(A)$, is the set of eigenvalues in the complex plane $\mathbb{C}$. Suppose we are seeking solutions proportional to $\exp(\sigma t)$. If $\sigma(A)$ does not protrude into the half-plane $\Re(z) > 0$ then the system is asymptotically stable. This is the case for the toy model but, as we have seen, there is significant transient growth that eigenvalue analysis cannot directly reveal. In order to show that an operator is non-normal we can use a generalization of the eigenvalue spectrum called the *ϵ-pseudospectrum*, or pseudospectrum for short (Trefethen and Embree, 2005).

Definition 1. Let A be an operator and let $\epsilon > 0$ be arbitrary. The ϵ-pseudospectrum $\sigma_\epsilon(A)$ of A is the set of $z \in \mathbb{C}$ such that

$$\|(zI - A)^{-1}\| > \epsilon^{-1}, \tag{48}$$

where I is the identity operator and $\|\cdot\|$ is a suitable norm.

The quantity $(zI - A)^{-1}$ is known as the *resolvent* of A. Clearly, when $z \in \sigma(A)$, the resolvent is not defined. It may, at first, seem that Definition 1 is not particularly useful since the norm of the resolvent is large when z is close to an eigenvalue. This is true for normal operators, with $\|\cdot\| = \|\cdot\|_2$. For non-normal operators, however, $\|(zI - A)^{-1}\|$ can be large even when z is far from the spectrum. The resolvent for the toy model has the analytical

expression

$$(zI - A)^{-1} = \begin{pmatrix} \dfrac{S}{zS+1} & 0 \\ \dfrac{S^2}{(zS+1)(zS+2)} & \dfrac{S}{zS+2} \end{pmatrix}. \tag{49}$$

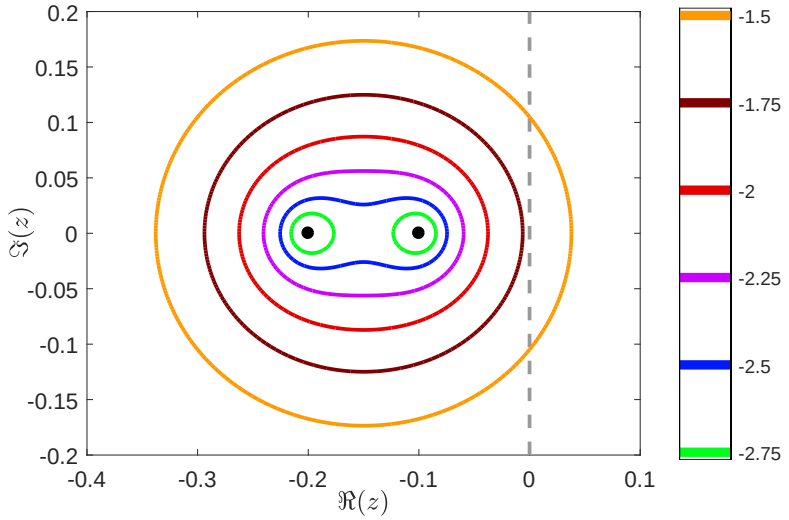

Figure 5. The spectrum and pseudospectra of A for $S = 10$. The solid dots represent the eigenvalues and the contours show the pseudospectra for $\epsilon = 10^{\beta}$, with different values of β displayed in the colour bar. The vertical dashed line indicates $\Re(z) = 0$.

Figure 5 displays contours of the L_2-norm of the resolvent in (49) for several values of ϵ. The contours in Figure 5 extend far from the eigenvalues. This fact tells us that transient growth could be important in this system. We can, however, use the information in Figure 5 to dig a little deeper. In normal mode analysis, we would look for

$$\alpha(A) = \sup_{z \in \sigma(A)} \Re(z), \tag{50}$$

which is known as the *spectral abscissa* of A (e.g. Trefethen and Embree, 2005). Clearly, $\alpha(A)$ is negative, indicating asymptotic stability. The pseu-

dospectrum contour corresponding to $\epsilon = 10^{-1.5}$ passes into the $\Re(z) > 0$ half of the plane and this fact gives useful information on the size of possible transient growth. To see how, consider the *pseudospectral abscissa*

$$\alpha_\epsilon(A) = \sup_{z \in \sigma_\epsilon(A)} \Re(z), \tag{51}$$

which is analogous to the definition of the spectral abscissa. The envelope of transient growth is $\| \exp(tA) \|_2$ for $t \geq 0$, as displayed in Figure 4. It can be shown (Trefethen and Embree, 2005) that the largest possible transient growth has a lower bound given by

$$\sup_{t \geq 0} \| \exp(tA) \|_2 \geq \frac{\alpha_\epsilon(A)}{\epsilon}, \ \forall \epsilon > 0. \tag{52}$$

Using the information from Figure 5, for $\epsilon = 10^{-1.5}$, $\alpha_\epsilon(A) = 3.78 \times 10^{-2}$ and a lower bound for the maximum transient growth is $\sup_{t \geq 0} \| \exp(tA) \|_2 \geq 1.196$. In short, the spectral abscissa reveals whether or not a linear system has exponential growth and the pseudospectral abscissa does the same but for transient growth.

There are several algorithms to calculate pseudospectra, with a comprehensive account given in Trefethen and Embree (2005). An excellent tool for investigating pseudospectra is `eigtool` (Wright, 2002). This software has been used to calculate the pseudospectra in this Chapter.

Eigenvalue sensitivity Another useful interpretation of pseudospectra is a definition based on the sensitivity of eigenvalues.

Definition 2. $\sigma_\epsilon(A)$ is the set of $z \in \mathbb{C}$ such that

$$z \in \sigma(A + E), \tag{53}$$

for some E with $\|E\| < \epsilon$.

The proof that definitions 1 and 2 are equivalent is given in Trefethen and Embree (2005). In this new definition we consider perturbing the eigenvalue problem, that is a perturbation operator of $O(\epsilon)$ is added to the system operator and the spectrum of the combined operators is calculated. If this were done for all such operators E, the region mapped out on the complex plane by all of these spectra is the pseudospectrum, i.e.

$$\sigma_\epsilon(A) = \bigcup_{\|E\| < \epsilon} \sigma(A + E). \tag{54}$$

In practice, we cannot calculate (54) exactly. However, it normally takes only a few different E to give a good indication whether or not an operator is non-normal. Figure 6 shows how the eigenvalues of the toy model, for $S = 1000$, jump to distances greater than $O(\epsilon)$ (i.e. the size of the perturbation) when the operator A is perturbed. The eigenvalues for fifty different E with $\|E\|_2 = O(10^{-6})$ are displayed. The eigenvalues of the perturbed operator

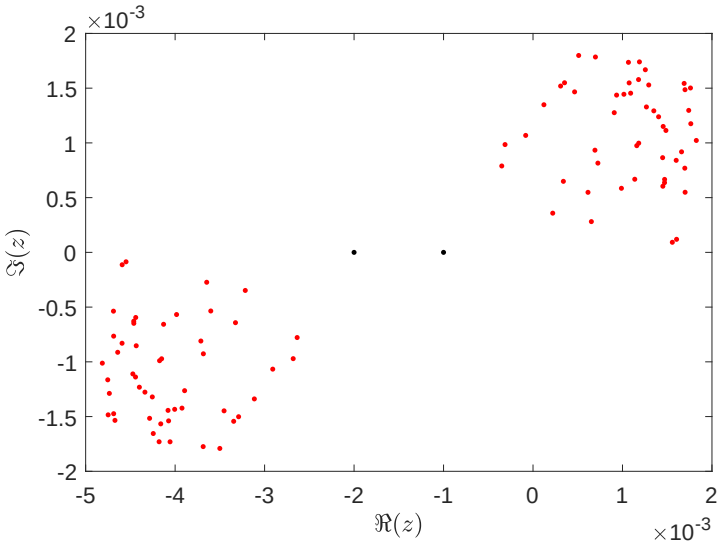

Figure 6. The eigenvalues of A (black dots) and the eigenvalues of 50 iterations of $A + E$ where $\|E\|_2 = O(10^{-6})$ (red dots). In this example, $S = 1000$.

jump three orders of magnitude greater than the size of the perturbation. This approach gives a quick indication of the non-normality of an operator. If A were normal, the perturbed eigenvalues would sit $O(\epsilon)$ away from the eigenvalues in the complex plane.

Choice of norm Before moving onto studying transient growth in the TI onset, it is important to point out that this analysis is dependent on the *choice of norm*. The general rule is to choose a norm that has a clear physical meaning. For the toy model, we have used the L_2-norm, which can be thought of as the "root mean square" of the perturbed quantities. Not only is this norm simple to use with a clear physical interpretation but many mathematical results are available for the L_2-norm concerning

psuedospectra. Changing the norm, however, can change the shape of pseudospectra (Trefethen, 1999; Trefethen and Embree, 2005) so norm selection must be treated with care. Another obvious choice is the energy norm (e.g. Reddy and Henningson, 1993; Schmid and Henningson, 1994; MacTaggart and Stewart, 2017; MacTaggart, 2018). Sometimes a suitable norm is evident from the analysis but for other applications, normally involving more detailed models, care must be taken in order to produce a "physically useful" norm (e.g. Hanifi et al., 1996).

Optimal perturbations Although large transient growth can occur in systems with non-normal operators, the size of the transient growth is dependent on the initial conditions. For the toy model, the envelopes of *maximum* transient growth are shown in Figure 4. But what initial perturbations give rise to the maximum transient growth? Suppose we wish to find the initial condition that gives rise to the maximum transient growth at time t_m for the toy model. If $\mathbf{q}_0$ represents this initial condition, we can write

$$B\mathbf{q}_0 = \mu\mathbf{q}_{t_m}, \tag{55}$$

where $\mathbf{q}_{t_m}$ denotes the evolved perturbation after a time t_m, $B = \exp(t_m A)$ and $\mu = \|\exp(t_m A)\|_2$. Since μ is the *largest singular value* of B, we can solve for the optimal initial condition $\mathbf{q}_0$ (and the resulting perturbation $\mathbf{q}_{t_m}$) by decomposing B into

$$BV = U\Sigma, \tag{56}$$

where U and V are unitary matrices and Σ is a diagonal matrix containing the singular values ordered by size.

If we focus on the columns $\mathbf{u}_1$ and $\mathbf{v}_1$, of U and V respectively, corresponding to the largest singular value, we have

$$B\mathbf{v}_1 = \mu_1\mathbf{u}_1, \tag{57}$$

where μ_1 represents the largest singular value. What equation (57) states is that an input vector $\mathbf{v}_1$ is mapped by B onto $\mathbf{u}_1$ stretched by a factor μ_1 (Schmid and Henningson, 2001).

For the toy model, the optimal initial conditions are just individual values as the system is based on a 2×2 matrix. For example, using the singular value decomposition (SVD) described above in equations (56) and (57), the optimal initial conditions giving rise to the maximum possible transient growth at $t = 40$ for $S = 60$ are $b = -0.9998$ and $j = -0.0176$.

3.2 Transient growth of the TI

The study of transient growth in the linear onset of instability has been well-developed for viscous shear flows (see Schmid and Henningson, 2001, and references therein). In order to link up with this previous catalogue of work, we extend the MHD model considered so far to include Newtonian viscosity. That is, the (non-dimensional) model equations are now

$$\frac{\partial \mathbf{u}}{\partial t} + (\mathbf{u}\cdot\boldsymbol{\nabla})\mathbf{u} = -\boldsymbol{\nabla} p + (\boldsymbol{\nabla}\times\mathbf{B})\times\mathbf{B} + \frac{1}{Re}\nabla^2\mathbf{u}, \tag{58}$$

$$\frac{\partial \mathbf{B}}{\partial t} = \boldsymbol{\nabla}\times(\mathbf{u}\times\mathbf{B}) + \frac{1}{S}\boldsymbol{\nabla}^2\mathbf{B}, \tag{59}$$

$$\boldsymbol{\nabla}\cdot\mathbf{B} = \boldsymbol{\nabla}\cdot\mathbf{u} = 0, \tag{60}$$

where Re is the Reynolds number and all other variables have their standard definitions. As well as an equilibrium magnetic field $\mathbf{B}_0 = B_{0z}(x)\mathbf{e}_z$, we now consider, in general, an equilibrium flow $\mathbf{u}_0 = U_{0z}(x)\mathbf{e}_z$. The equilibrium equations become

$$\mathbf{0} = -\boldsymbol{\nabla} p_0 + (\boldsymbol{\nabla}\times\mathbf{B}_0)\times\mathbf{B}_0 + \frac{1}{Re}\boldsymbol{\nabla}^2\mathbf{u}_0, \tag{61}$$

$$\mathbf{0} = \boldsymbol{\nabla}\times(\mathbf{u}_0\times\mathbf{B}_0). \tag{62}$$

Clearly, for the assumed forms of the equilibrium magnetic and velocity fields, equation (62) is satisfied. Once $\mathbf{u}_0$ and $\mathbf{B}_0$ are chosen, the background pressure p_0 is determined from equation (61). Again, we ignore the effect of magnetic diffusion on the equilibrium magnetic field.

Linearizing equations (58) to (60) and seeking solutions of the form (14), leads to

$$\frac{\partial}{\partial t}(D^2-k^2)u = L_B b - L_U u + \frac{1}{Re}(D^2-k^2)^2 u, \tag{63}$$

$$\frac{\partial b}{\partial t} = ik(B_{0z}u + U_{0z}b) + \frac{1}{S}(D^2-k^2)b, \tag{64}$$

where

$$L_U = ik[U_{0z}(D^2-k^2) - U_{0z}''], \quad L_B = ik[B_{0z}(D^2-k^2) - B_{0z}''], \quad D = \partial/\partial x, \tag{65}$$

and the prime refers to differentiation with respect to x in the background equilibrium fields.

As before, we consider no-slip and perfectly conducting boundary conditions,

$$u = Du = b = 0 \text{ at } x = \pm d, \tag{66}$$

where the extra condition $Du = 0$ enters since equation (63) is fourth order.

General approach We will now describe an approach for investigating transient growth in the system (63) and (64) which is an extension of that described for the toy model. First, we rewrite equations (63) and (64) in the form

$$\frac{\partial}{\partial t} M\mathbf{v} = L\mathbf{v}, \tag{67}$$

where $\mathbf{v} = (u, b)^T$,

$$M = \begin{pmatrix} D^2 - k^2 & 0 \\ 0 & I \end{pmatrix}, \tag{68}$$

$$L = \begin{pmatrix} \frac{1}{Re}(D^2 - k^2)^2 - L_U & L_B \\ ikB_{0z} & ikU_{0z} + \frac{1}{S}(D^2 - k^2) \end{pmatrix}, \tag{69}$$

and I represents the identity operator.

From the toy model, we found that transient growth is related to the non-orthogonality of the eigenfunctions. Therefore, we will make use of this fact and build our solution using eigenfunctions that contribute transient growth. To do this, we must first convert the initial value problem (67) into an eigenvalue problem. Consider the form

$$\mathbf{v} = \widetilde{\mathbf{v}} \exp(\sigma t), \tag{70}$$

where $\widetilde{\mathbf{v}}$ is an eigenfunction and σ the corresponding eigenvalue. The generalized eigenvalue problem is, therefore,

$$\sigma M\widetilde{\mathbf{v}} = L\widetilde{\mathbf{v}}. \tag{71}$$

One often overlooked property related to the eigenfunction expansions concerning the TI is the completeness of the eigenfunctions. We pick up on this point in the Appendix.

Once (71) is solved, we must select a subset of eigenfunctions to consider. We can use pseudospectra to help us select the eigenfunctions that will contribute to large transient growth. For the moment, however, let us assume that the selection of N eigenfunctions has been made and that we restrict ourselves to a subspace spanned by these eigenfunctions,

$$\mathbb{S}^N = \{\widetilde{\mathbf{v}}_1, \ldots, \widetilde{\mathbf{v}}_N\}. \tag{72}$$

We expand vector functions $\mathbf{v} \in \mathbb{S}^N$ in terms of the basis $\{\widetilde{\mathbf{v}}_1, \ldots, \widetilde{\mathbf{v}}_N\}$,

$$\mathbf{v} = \sum_{i=1}^{N} \kappa_i(t)\widetilde{\mathbf{v}}_i. \tag{73}$$

Notice that the coefficients κ_i are functions of t since we will solve the full problem (67) rather than just the eigenvalue problem (71).

Using equation (73), we can restate equation (67) in the form

$$\frac{\mathrm{d}\boldsymbol{\kappa}}{\mathrm{d}t} = \Lambda\boldsymbol{\kappa}, \quad \Lambda \in \mathbb{C}^{N\times N}, \quad \boldsymbol{\kappa} \in \mathbb{C}^N, \tag{74}$$

with

$$\boldsymbol{\kappa} = [\kappa_1, \ldots, \kappa_N]^T, \quad \Lambda = \mathrm{diag}[\sigma_1, \ldots, \sigma_N]. \tag{75}$$

The operator Λ represents the linear evolution operator $M^{-1}L$ projected onto the subspace $\mathbb{S}^N$.

For our disturbance measure, let us consider the disturbance kinetic and magnetic energies, i.e.

$$E_V = \frac{1}{2}\int_V \left(|\mathbf{u}|^2 + |\mathbf{b}|^2\right)\,\mathrm{d}V. \tag{76}$$

By making use of the solenoidal constraints $(8)_1$ and $(8)_2$, it can be shown (e.g. MacTaggart and Stewart, 2017) that, for a given k, the energy density can be written as

$$E = \frac{1}{2k^2}\int_{-d}^{d} \left(|Du|^2 + k^2|u|^2 + |Db|^2 + k^2|b|^2\right)\,\mathrm{d}x, \tag{77}$$

which represents the energy disturbance measure for a given k. Hence, we define the energy norm as

$$\|\mathbf{v}\|_E^2 = \frac{1}{2k^2}\int_{-d}^{d} \left(|Du|^2 + k^2|u|^2 + |Db|^2 + k^2|b|^2\right)\,\mathrm{d}x. \tag{78}$$

For any $\mathbf{v}_1$, $\mathbf{v}_2 \in \mathbb{S}^N$, the inner product associated with the above energy norm can be written as

$$(\mathbf{v}_1, \mathbf{v}_2)_E = \frac{1}{2k^2}\int_{-d}^{d} \mathbf{v}_1^H \mathcal{Q}\mathbf{v}_2\,\mathrm{d}x, \tag{79}$$

where

$$\mathcal{Q} = \begin{pmatrix} k^2 - D^2 & 0 \\ 0 & k^2 - D^2 \end{pmatrix}. \tag{80}$$

The superscript H denotes the complex-conjugate transpose.

For calculations, it will be convenient to work with the L_2-norm rather than the energy norm so we can make use of the SVD approach described above. First, let us rewrite equation (79) as

$$(\mathbf{v}_1, \mathbf{v}_2)_E = \boldsymbol{\kappa}_1^H Q\boldsymbol{\kappa}_2, \tag{81}$$

where the matrix Q has components

$$Q_{ij} = (\widetilde{\mathbf{v}}_i, \widetilde{\mathbf{v}}_j)_E = \frac{1}{2k^2} \int_{-d}^{d} \widetilde{\mathbf{v}}_i^H \mathcal{Q} \widetilde{\mathbf{v}}_j \, \mathrm{d}x. \tag{82}$$

Since Q is both Hermitian and positive-definite, we can write $Q = F^H F$. Using this factorization, we can write

$$\begin{aligned} (\mathbf{v}_1, \mathbf{v}_2)_E &= \boldsymbol{\kappa}_1 Q \boldsymbol{\kappa}_2, \\ &= \boldsymbol{\kappa}_1^H F^H F \boldsymbol{\kappa}_2, \\ &= (F\boldsymbol{\kappa}_1, F\boldsymbol{\kappa}_2)_2. \end{aligned} \tag{83}$$

The associated vector norm is

$$\|\mathbf{v}\|_E = \|F\boldsymbol{\kappa}\|_2, \quad \mathbf{v} \in \mathbb{S}^N. \tag{84}$$

We are now in a position to determine the optimal transient growth envelope for the TI onset as we did for the toy model in equation (42). The formal solution of the initial value problem (67) can be written as

$$\mathbf{v}(t) = \exp(M^{-1}Lt)\mathbf{v}_0, \quad \mathbf{v}_0 = \mathbf{v}(0), \tag{85}$$

in the primitive variables and as

$$\boldsymbol{\kappa}(t) = \exp(\Lambda t)\boldsymbol{\kappa}_0, \quad \boldsymbol{\kappa}_0 = \boldsymbol{\kappa}(0), \tag{86}$$

in the new variables introduced in this section. Using these expressions, the optimal energy growth envelope is found to be

$$\begin{aligned} G(t) &= \sup_{\mathbf{v}_0 \neq 0} \frac{\|\mathbf{v}(t)\|_E^2}{\|\mathbf{v}_0\|_E^2} \\ &= \sup_{\boldsymbol{\kappa}_0 \neq 0} \frac{\|F\boldsymbol{\kappa}(t)\|_2^2}{\|F\boldsymbol{\kappa}_0\|_2^2} \\ &= \sup_{\boldsymbol{\kappa}_0 \neq 0} \frac{\|F\exp(\Lambda t)\boldsymbol{\kappa}_0\|_2^2}{\|F\boldsymbol{\kappa}_0\|_2^2} \\ &= \sup_{\boldsymbol{\kappa}_0 \neq 0} \frac{\|F\exp(\Lambda t)F^{-1}F\boldsymbol{\kappa}_0\|_2^2}{\|F\boldsymbol{\kappa}_0\|_2^2} \\ &= \|F\exp(\Lambda t)F^{-1}\|_2^2. \end{aligned} \tag{87}$$

Building $\mathbb{S}^N$ Before discussing the behaviour of transient growth at the onset of the TI, we must first consider which eigenfunctions to include in the subspace $\mathbb{S}^N$. To answer this, we must consider the shape of the eigenvalue spectrum. In what follows, the equilibrium magnetic field will be the Harris sheet (17), i.e. $B_{0z}(x) = \tanh(x)$, and the equilibrium velocity field will be zero, i.e. $U_{0z}(x) = 0$. Taking the parameters $d = 15$, $k = 0.5$, $S = 10^3$ and $Re = 10^6$, the eigenvalue spectrum is displayed in Figure 7 for eigenvalues with $\Re(\sigma) > -k$. The eigenvalues in Figure 7 have been determined by solving (71) with a pseudospectral discretization of the differential equations (MacTaggart, 2018).

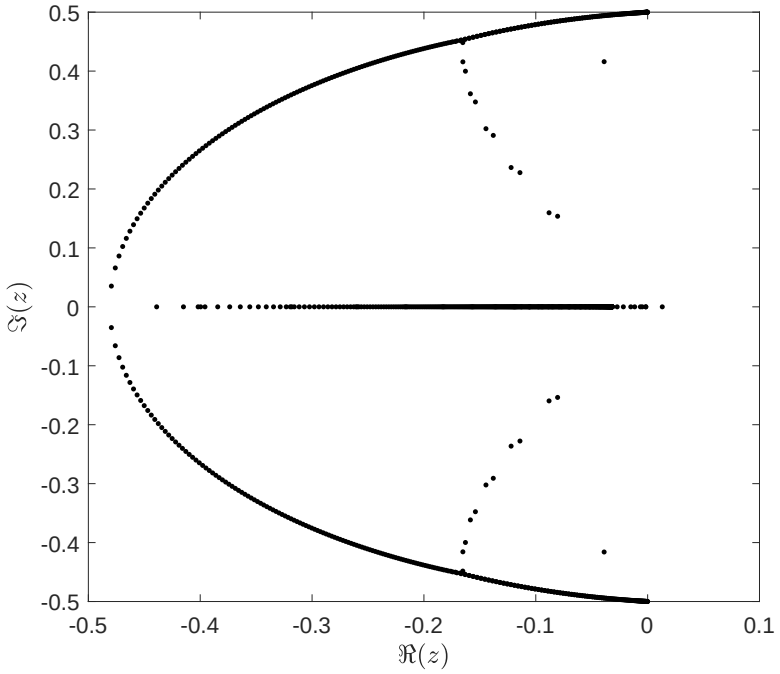

Figure 7. The eigenvalue spectrum for the projection keeping eigenvalues with $\Re(\sigma) > -k$.

There are several elements to notice in this spectrum. The first is that there is one eigenvalue satisfying $\Re(\sigma) > 0$. This eigenvalue is associated with the *tearing mode*, the unique unstable eigenfunction of the TI onset

problem. All the other eigenvalues satisfy $\Re(\sigma) < 0$ (i.e. asymptotic damping) and exhibit a branching structure. Beyond $\Re(z) = -k$, in the negative direction, the central branch of eigenvalues continues and no new branches are created.

The branching of eigenvalues is usually an indicator of non-normality in the underlying operators (e.g. Reddy et al., 1993). It can be shown that if $\mathbb{S}^N$ contains eigenfunctions associated with the eigenvalues at the branch points, much higher transient growth is possible than if they were not included (MacTaggart, 2018). Such behaviour is indicated from the pseudospectra in Figure 8. The strongest deviation of the contours is at the connecting branches. The green contour is deflected by ~ 0.1 but has $\epsilon = 10^{-8}$. For a normal operator, the resulting deflection would be $O(10^{-8})$ but here the deflection is seven orders of magnitude greater thanks to non-normality.

A contour is also displayed entering the half plane $\Re(z) > 0$, as for the toy model. Although the eigenvalue of the tearing mode has been included in Figure 8, its removal does not change this result. Therefore, based on the bound in (52), we can expect transient growth. In short, when building $\mathbb{S}^N$, it is vital to include the eigenfunctions corresponding to the eigenvalues at the branch points in the spectrum since these will contribute the largest transient growth.

Energy growth behaviour In order to demonstrate how the optimal energy growth is affected by the inclusion of asymptotically damped eigenfunctions, we perform the optimization problem and compare the cases where $\mathbb{S}^N$ includes (a) the tearing mode and other damped eigenfunctions, and (b) the tearing mode alone. For the parameters $S = 10^3$, $Re = \infty$ (i.e. an inviscid fluid) and $k = 0.2$, Figure 9 shows the optimal energy growth envelopes for the two cases. Focussing on the dashed curve in Figure 9, this corresponds to the optimal energy growth due to the tearing mode alone. The tearing mode grows exponentially in the linear problem and since $\log G(t)$ is plotted on the y-axis, this curve is a straight line. The solid line shows the optimal growth envelope calculated with eigenfunctions whose eigenvalues satisfy $\Re(\sigma) > -0.6$. What is clear is that the maximum possible energy growth at small times is significantly larger than what would be predicted using the tearing mode alone. At later times, the solid curve becomes parallel to the dashed curve. This is because the transient behaviour has decayed and the tearing mode dominates the linear growth. Even at later times, however, the effect of the transient growth can still be felt. At $t = 100$, for this set of parameters, asymptotic stability analysis would predict a maximum possible energy amplification of ~ 30. Including damped eigenfunctions in

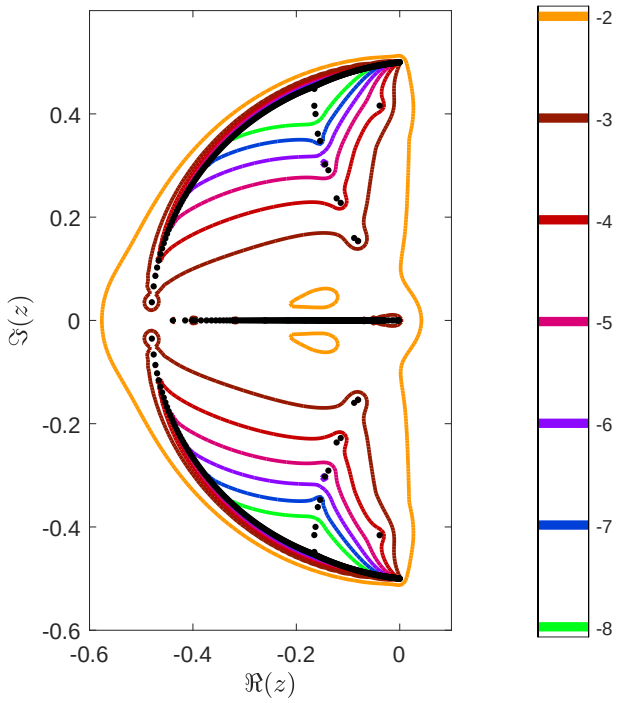

Figure 8. The spectrum from Figure 7 with pseudospectrum contours included. Each contour has $\epsilon = 10^n$, where the range of n is displayed in the colour bar.

the calculation, the maximum possible energy amplification is ~ 400.

In the toy model, we found that the maximum possible growth depended heavily on S. The same is true for the TI onset. Figure 10 displays the optimal energy growth envelopes for different S and parameters $k = 0.5$ and $\Re(\sigma) > -k$. Time has been scaled by $S^{1/2}$ as the tearing mode begins to dominate the linear growth at $t \sim O(S^{1/2})$ (Borba et al., 1994). Therefore, after $t/S^{1/2} \sim 1$, the exponential growth of the tearing mode becomes more visible.

This scaling of time also reveals that as S increases, the maximum possible energy growth due to transients (i.e. the growth at early times) also increases. This result appears to be robust for both tearing-unstable

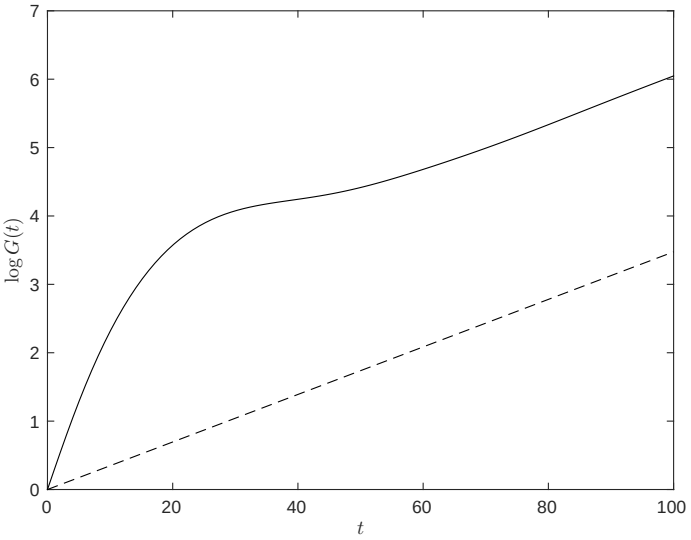

Figure 9. Optimal energy growth envelopes for $\Re(\sigma) > -0.6$ (solid line) and $\Re(\sigma) > 0$ (dashed line).

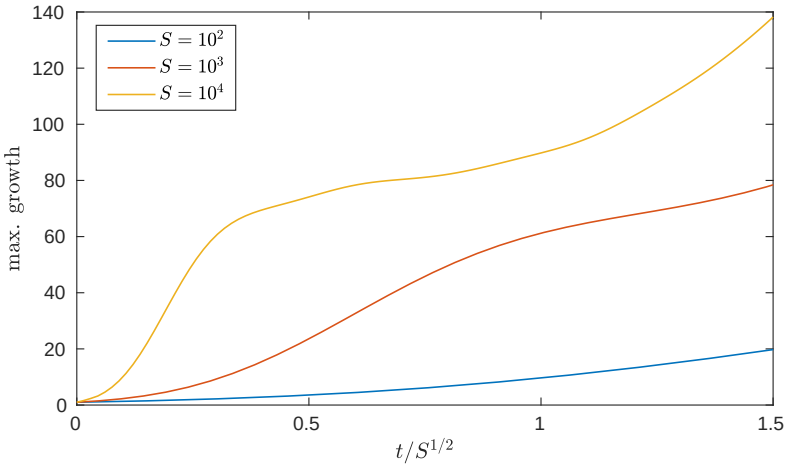

Figure 10. Optimal energy growth envelopes for various S with $k = 0.5$ and $\Re(\sigma) > -k$.

($0 < k < 1$) and tearing-stable ($k > 1$) wavenumbers (MacTaggart and Stewart, 2017; MacTaggart, 2018). Also, this result is true in other disturbance measures. For example, MacTaggart (2018) finds that, optimizing with respect to the L_2-norm (as we did for the toy model) whilst excluding the tearing mode from the calculation, the maximum possible transient growth scales as $O(S^{1/4})$ in a time of $O(S^{1/4})$ for $0 < k < 1$. Again, this result indicates the possibility of significant growth long before the tearing mode dominates the linear behaviour.

Optimal initial conditions In the above descriptions of transient growth, we have been careful to describe the maximum *possible* transient growth. This qualification is important as transient growth is *dependent* on the initial condition. This behaviour differs from asymptotic stability, which does not read the form of the (infinitesimal) initial condition.

Applying the SVD, as described earlier for the toy model, Figure 11 displays the optimal initial conditions for u and b when $S = 10^4$ and $t = 50$ and optimization is performed with respect to the L_2-norm (MacTaggart, 2018). Notice that the initial conditions in Figure 11 take the form of *wave packets* in the current sheet. Such forms can be related to the theory of *pseudomodes* (Trefethen and Embree, 2005) which are a generalization of eigenfunctions in the similar way as pseudospectra are a generalization of spectra. What is important to notice, however, is that the optimal initial conditions can be represented as *noise in the current sheet* - something likely to be present in high-S applications of the TI.

A Completeness

Since the *completeness* of eigenfunctions is a vital property for the stability analysis we have discussed, we now say a few words about it here. In the fluid dynamics literature, one popular reference related to proving the completeness of the eigenfunctions of non-self-adjoint eigenvalue problems is DiPrima and Habetler (1969). In the theorem of DiPrima and Habetler (1969), the operators of the eigenvalue problem are written as

$$\sigma M\mathbf{v} = L\mathbf{v} = (L_s + B)\mathbf{v}. \tag{88}$$

L_s is a self-adjoint operator and B is a 'perturbation' (that is, whatever remains). The order of the derivatives in B must be lower than those in L_s since B is a perturbation. If we can express the eigenvalue problem for the onset of the TI in the form of equation (88), we can use the theorem of DiPrima and Habetler (1969) to prove that the eigenfunctions are complete.

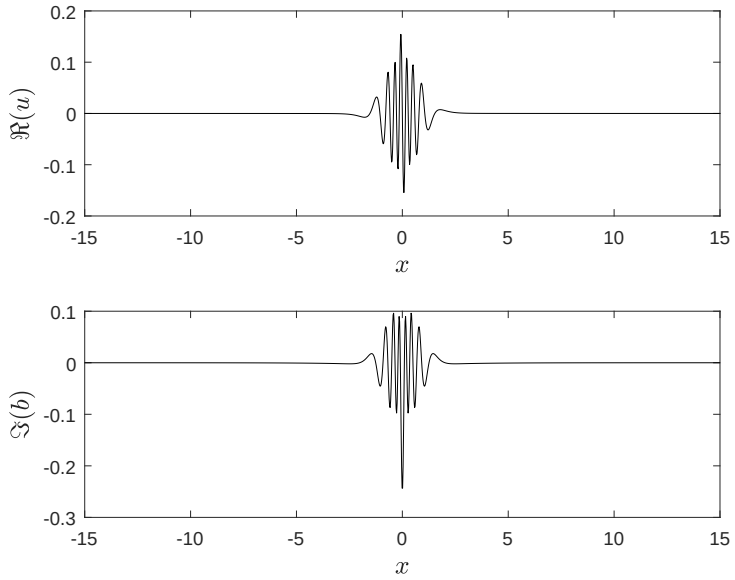

Figure 11. The initial conditions that produce optimal transient growth at $t = 50$ for $S = 10^4$.

As they stand, equations (63) and (64) are not in a suitable form for this $L_s + B$ split. In order to achieve a suitable split, we must reconsider how we linearize the MHD equations. Until now, we have linearized the curl of the momentum equation (in order to eliminate the pressure) but have linearized the induction equation directly. If, instead, we also take the curl of the induction equation and linearize this, we find

$$\begin{aligned}\frac{\partial}{\partial t}(D^2 - k^2)b &= ik[B_0(D^2 - k^2) + B_0'']u - ik[U_0(D^2 - k^2) + U_0'']b \\ &\quad +2ik(B_0'Du - U_0'Db) + \frac{1}{S}(D^2 - k^2)^2 b. \end{aligned} \tag{89}$$

After some algebraic manipulation, we achieve an eigenvalue problem suitable for the theorem of DiPrima and Habetler (1969):

$$\lambda M\mathbf{v} = L\mathbf{v} = (L_s + B)\mathbf{v}, \tag{90}$$

where $\lambda = -\sigma$, $\mathbf{v} = (u, b)^T$,

$$M = \begin{pmatrix} -D^2 + k^2 & 0 \\ 0 & -D^2 + k^2 \end{pmatrix}, \tag{91}$$

$$L_s = \begin{pmatrix} \frac{1}{Re}(-D^2 + k^2)^2 & 0 \\ 0 & \frac{1}{S}(-D^2 + k^2)^2 \end{pmatrix}, \tag{92}$$

and

$$B = \begin{pmatrix} \mathcal{L}_U^+ & -\mathcal{L}_B^+ \\ -\mathcal{L}_B^- + 2ikB_{0z}{}'D & \mathcal{L}_U^- - 2ikU_{0z}{}'D \end{pmatrix}, \tag{93}$$

where

$$\mathcal{L}_U^\pm = ik[U_{0z}(-D^2 + k^2) \pm U_0''] \quad \text{and} \quad \mathcal{L}_B^\pm = ik[B_{0z}(-D^2 + k^2) \pm B_0'']. \tag{94}$$

Now the operators in B are of lower order compared to those L_s and this representation is suitable for the application of the theorem of DiPrima and Habetler (1969), proving completeness of the eigenfunctions.

Since we have increased the order of the induction equation, we need to add extra boundary conditions to complete the mathematical description of the problem. The suitable extra boundary conditions in this case are

$$Db = 0 \quad \text{at} \quad x = \pm d. \tag{95}$$

These conditions derive from the solenoidal constraint $(60)_1$ in the same way that the $Du = 0$ conditions derive from the incompressibility condition $(60)_2$.

Bibliography

A. Bhattacharjee, Y.-M. Huang, H. Yang, and B. Rogers. Fast reconnection in high-lundquist-number plasmas duee to the plasmoid instability. *Physics of Plasmas*, 16:112102, 2009.

J. Birn and M. Hesse. Geospace Environmental Modeling (GEM) magnetic reconnection challenge: Resistive tearing, anisotropic pressure and Hall effects. *Journal of Geophysical Research*, 106:3737–3750, 2001.

J. Birn and E.R. Priest, editors. *Reconnection of magnetic fields: magnetohydrodynamics and collisionless theory and observations*, 2007. Cambridge University Press.

J. Birn, J.F. Drake, M.A. Shay, B.N. Rogers, R.E. Denton, M. Hesse, M. Kuznetsova, Z.W. Ma, A. Bhattacharjee, A. Otto, and P.L. Pritchett. Geospace Environmental Modeling (GEM) Magnetic Reconnection Challenge. *Journal of Geophysical Research*, 106:3715–3719, 2001.

D. Biskamp. Magnetic reconnection in current sheets. *Physics of Fluids*, 29:1520–1531, 1986.

D. Biskamp. *Nonlinear magnetohydrodynamics*. Cambridge University Press, 1993.

D. Borba, K.S. Riedel, W. Kerner, G.T.A. Huysmans, M. Ottaviani, and P.J. Schmid. The pseudospectrum of the resistive magnetohydrodynamics operator: Resolving the resistive Alfvén paradox. *Physics of Plasmas*, 1:3151–3160, 1994.

D. Del Sarto, F. Pucci, A. Tenerani, and M. Velli. "Ideal" tearing and the transition to fast reconnection in the weakly collisional MHD and EMHD regimes. *Journal of Geophysical Research*, 121:1857–1873, 2016.

R. C. DiPrima and G.J. Habetler. A completeness theorem for non-selfadjoint eigenvalue problems in hydrodynamic stability. *Archive for Rational Mechanics*, 34:218–227, 1969.

D. Dobrott, S.C. Prager, and J.B. Taylor. Influence of diffusion on the resistive tearing mode. *Physics of Fluids*, 20:1850–1854, 1977.

W. Eckhaus. *Matched Asymptotic Expansions and Singular Perturbations*. North-Holland Publishing Company, 1973.

T.G. Forbes and E.R. Priest. A numerical experiment relevant to the line-tied reconnection in two-ribbon flares. *Solar Physics*, 84:169–188, 1983.

H.P. Furth, J. Killeen, and M. Rosenbluth. Finite-Resistivity Instabilities of a Sheet Pinch. *Physics of Fluids*, 6:459–484, 1963.

J.P. Goedbloed, R. Keppens, and S. Poedts. *Advanced Magnetohydrodynamics*. Cambridge University Press, 2010.

A. Hanifi, P.J. Schmid, and D.S. Henningson. Transient growth in compressible boundary layer flow. *Physics of Fluids*, 826:826–837, 1996.

E.G. Harris. On a plasma sheath separating regions of oppositely directed magnetic field. *Nuovo Cimento*, 23:115–121, 1962.

Y.M. Huang, L. Comisso, and A. Bhattacharjee. Plasmoid instability in evolving current sheets and onset of fast reconnection. *Astrophysical Journal*, 849(75), 2017.

L. Janicke. Resistive tearing mode in weakly two-dimensional neutral sheets. *Physics of Fluids*, 23:1843–1849, 1980.

A.D. Jette. Force-Free Magnetic Fields in Resistive Magnetohydrostatics. *Journal of Mathematical Analysis and Applications*, 29:109–122, 1970.

R.M. Kulsrud. Magnetic reconnection: Sweet-Parker versus Petschek. *Earth, Planets and Space*, 53:417–422, 2001.

A. Lazarian and E.T. Vishniac. Reconnection in a weakly stochastic field. *Astrophysical Journal*, 517:700–718, 1999.

A. Lazarian, G. Eyink, E.T. Vishniac, and G. Kowal. Turbulent reconnection and its implications. *Philosophical Transactions of the Royal Society A*, 373(2041), 2015.

N.F. Loureiro, A.A. Schekochihin, and S.C. Cowley. Instability of current sheets and formation of plasmoid chains. *Physics of Plasmas*, 14(100703), 2007.

N.F. Loureiro, D.A. Uzdensky, A.A. Schekochihin, S.C. Cowley, and T.A. Yousef. Turbulent magnetic reconnection in two dimensions. *Monthly Notices of the Royal Astronomical Society*, 399:L146–L150, 2009.

D. MacTaggart. The non-modal onset of the tearing instability. *Journal of Plasma Physics*, 84:905840501, 2018.

D. MacTaggart and P. Stewart. Optimal energy growth in current sheets. *Solar Physics*, 292(148), 2017.

W.A. Newcomb. Motion of magnetic lines of force. *Annals of Physics*, 3: 347–385, 1958.

R. B. Paris. Resistive instabilities in MHD. *Annales de Physique*, 9:374–432, 1984.

E.N. Parker. Acceleration of Cosmic Rays in Solar Flares. *Physical Review*, 107:830–836, 1957a.

E.N. Parker. Sweet's mechanism for merging magnetic fields in conducting fluids. *Journal of Geophysical Research*, 62:509–520, 1957b.

H.E. Petschek. Magnetic field annihilation. In *The Physics of Solar Flares, Proceedings of the AAS-NASA Symposium (Goddard Space Flight Center 1963)*, pages 425–439, 1964.

E. R. Priest. Magnetic theories of solar flares. *Solar Physics*, 86:33–45, 1983.

E.R. Priest and T. Forbes. *Magnetic reconnection: MHD theory and applications*. Cambridge University Press, 1993.

F. Pucci and M. Velli. Reconnection of quasi-singular current sheets: the "ideal" tearing mode. *Astrophysical Journal Letters*, 780(L14), 2014.

F. Pucci, M. Velli, A. Tenerani, and D. Del Sarto. Onset of fast "ideal" tearing in thin current sheets:Dependence on the equilibrium current profile. *Physics of Plasmas*, 25(032113), 2018.

S.C. Reddy and D.S. Henningson. Energy growth in viscous channel flows. *Journal of Fluid Mechanics*, 252:209–238, 1993.

S.C. Reddy, P.J. Schmid, and D.S. Henningson. Pseudospectra of the Orr-Sommerfield Operator. *SIAM Journal on Applied Mathematics*, 53:15–47, 1993.

R. Samtaney, N.F. Loureiro, D.A. Uzdensky, A.A. Schekochihin, and S.C. Cowley. Formation of plasmoid chains in magnetic reconnection. *Physical Review Letters*, 103:105004, 2009.

K. Schindler. *Physics of Space Plasma Activity*. Cambridge University Press, 2006.

P. Schmid and D.S. Henningson. *Stability and transition in shear flows*. Springer, 2001.

P.J. Schmid and D.S. Henningson. Optimal energy density growth in Hagen-Poiseuille flow. *Journal of Fluid Mechanics*, 277:197–255, 1994.

K. Shibata and S. Tanuma. Plasmoid-induced-reconnection and fractal reconnection. *Earth, Planets and Space*, 53:473–482, 2001.

R.S. Steinolfson and G. van Hoven. Nonlinear evolution of the resistive tearing mode. *Physics of Fluids*, 27:1207–1214, 1984.

P.A. Sweet. The neutral point theory of solar flares. In *IAU Symposium No. 6 Electromagnetic Phenomena in Ionized Gases (Stockholm 1956)*, page 123, 1958.

A. Tenerani, A.F. Rappazzo, M. Velli, and F. Pucci. The tearing mode instability of thin current sheets: the transition to fast reconnection in the presence of viscosity. *Astrophysical Journal*, 801(145), 2015.

T. Terasawa. Hall current effect on tearing mode instability. *Geophysical Research Letters*, 10:475–478, 1983.

L.N. Trefethen. Computation of pseudospectra. *Acta Numerica*, 8:247–295, 1999.

L.N. Trefethen and M. Embree. *Spectra and pseudospectra: the behaviour of nonnormal matrices and operators*. Princeton University Press, 2005.

L.N. Trefethen, A.E. Trefethen, S.C. Reddy, and T.A. Driscoll. Hydrodynamic stability without eigenvalues. *Science*, 261:578–584, 1993.

D.A. Uzdensky and N.F. Loureiro. Magnetic reconnection onset via disruption of a forming current sheet by the tearing instability. *Physical Review Letters*, 116(105003), 2016.

M.D. Van Dyke. *Perturbation methods in fluid mechanics*. Parabolic Press, 1975.

T.G. Wright. *Eigtool*. `http://www.comlab.ox.ac.uk/pseudospectra/eigtool`, 2002.